SPIN
Vol. 4, No. 2 (2014) 1440015 (6 pages)

DOI: 10.1142/S2010324714400153

World Scientific
www.worldscientific.com

HIGH-FREQUENCY MAGNETOCAPACITANCE EFFECT IN ORGANIC SPIN VALVE WITH A 3,4,9,10-PERYLENE-TERACARBOXYLIC-DIANHYDRIDE SPACER

JHEN-YONG HONG and SHENG-HONG CHEN
Department of Physics
National Taiwan University
10617 Taipei, Taiwan

WEN-CHUNG CHIANG
Department of Optoelectric Physics
Chinese Culture University
11114 Taipei, Taiwan

MINN-TSONG LIN*
Department of Physics
National Taiwan University
10617 Taipei, Taiwan

Institute of Atomic and Molecular Sciences
Academia Sinica, 10617 Taipei, Taiwan
**mtlin@phys.ntu.edu.tw*

Received 6 June 2014
Accepted 30 July 2014
Published 5 September 2014

The frequency-dependent impedance of a series of ferromagnet (FM)/organic semiconductor (OSC)/FM tri-layered organic spin valves (OSV) is investigated in the frequency range of 10 Hz–1 MHz. An equivalent resistor–capacitor (RC) parallel network model is employed to analyze the magnetoresistance (MR) and magnetocapacitance (MC) effects. Fitting with the model yields field-dependent parameters and the resistive parameters agree with the experimental results. The analysis of the impedance spectra indicates an effective magnetotransport mechanism dominated by the charge accumulation at the organic–FM interfaces.

Keywords: Organic spin valve; magnetoresistance; magnetocapacitance; organic semiconductor; impedance spectroscopy.

*Corresponding author.

1. Introduction

Organic semiconductors (OSCs) are promising materials for spintronics with novel properties that are not seen in conventional inorganic semiconductors. While the launch of OSC greatly enhances the versatility of modern photonic devices such as organic light-emitting diodes (OLED)[1,2] and organic photovoltaic (OPV) cells,[3,4] the efficiency of the devices is still a technical concern. On top of the working principle that controls the charge of the carriers, the control of the spin degree of freedom in OSCs has been much discussed because of the possibility of bringing new functionalities into organic electronics which in turn would improve the device performance. For example, by manipulating the spin of the injected carriers in OSC, spin-polarized OLED (spin-OLED) is predicted to have higher level of energy efficiency than OLED.[5–9] In order to realize spin phenomena-related organic devices, the ability to manipulate spin, including the injection and transport of spin polarization into the active layer, is of great technological interest.[10–13]

Although significant success has been achieved in controlling the magneto-response based on magnetoresistance (MR) effect in organic spin valves (OSV) consisting of two ferromagnetic (FM) electrodes separated by a thin organic spacer,[10–13] the magnetocapacitance (MC) effect, a phenomenon useful for characterizing some important physical properties such as dielectric and transport properties in spintronic devices, is less discussed and is worthy of further exploration. For example, AC magnetotransport has been proposed as a tool to study spin-dependent potentials, dielectric relaxation and high-frequency magnetic sensing.[14–17] The product of resistance and capacitance (the RC time constant) of a magnetic tunnel junction (MTJ) has been suggested for characterizing the high-speed performance of devices such as hard disk drive read heads and magnetic random access memories.[18–22] In addition, MC serves as an alternative approach for characterizing the interfacial properties within the OSV structure. Like other magneto-effects in organic or inorganic devices,[23,24] MC is predominately interface-driven also. The study of MC response in OSVs should therefore facilitate a better understanding of spin-dependent transport via the FM/OSC interfaces.

In this paper, we address the magneto-impedance properties of 3,4,9,10-perylene-teracarboxylic-dianhydride (PTCDA)-based OSVs. Both MR and MC effects are demonstrated in these OSVs with various PTCDA barrier thicknesses. The impedance spectra are fitted to an equivalent-circuit model consisting of a parallel resistor and capacitor network. The study suggests that the magnetotransport of PTCDA-based OSVs is dominated by spin accumulation at the FM/OSC interfaces.

2. Experiment

The PTCDA OSVs were grown on glass substrates and stacked from bottom to top in the following sequence: NiFe (30 nm)/CoFe (15 nm)/AlO_x (0.6 nm)/PTCDA (t_p, in nm)/AlO_x (0.6 nm)/CoFe (35 nm). In between the OSC PTCDA spacer and the neighboring CoFe layers, a thin, partially oxidized alumina layer is inserted, as shown schematically in Fig. 1(a). The insertion of alumina was to protect PTCDA from direct contact with the electrode material which would otherwise hybridize (through chemical reaction or inter-diffusion) at the interfaces and devastate the MR effect, as demonstrated in our previous works.[13,25] The whole sample stack was prepared in a high-vacuum environment with a base pressure of lower 10^{-8} mbar. All metallic layers were made by sputtering in an Ar working pressure of 5×10^{-3} mbar at the power of 20 W, and the organic PTCDA layer was grown at 10^{-8} mbar by thermal evaporation at a deposition rate of 0.1 nm/s. The spin valve structure was patterned by a shadow mask-changing sequence, and the junction area ($200 \times 200\,\mu m^2$) was defined by the intersection of the crossed electrodes. The current-perpendicular-to-the-plane (CPP) MR measurements were carried out at room temperature using the conventional DC four-point-probe method, whereas the impedance characterization was made by the AC two-terminal auto balancing bridge method at frequencies ranging from 10 Hz to 1 MHz using an Agilent HP 4294A Precision Analyzer, followed by an RC equivalent-circuit simulation. The variation of the fitted capacitive parameters with external magnetic field defines the MC.

3. Results and Discussion

3.1. *Magnetoresistance*

Figure 1(b) shows the cycling of the junction resistance with field at room temperature for a series of PTCDA-based OSVs with various PTCDA thicknesses t_P. The curve displays the typical pseudo

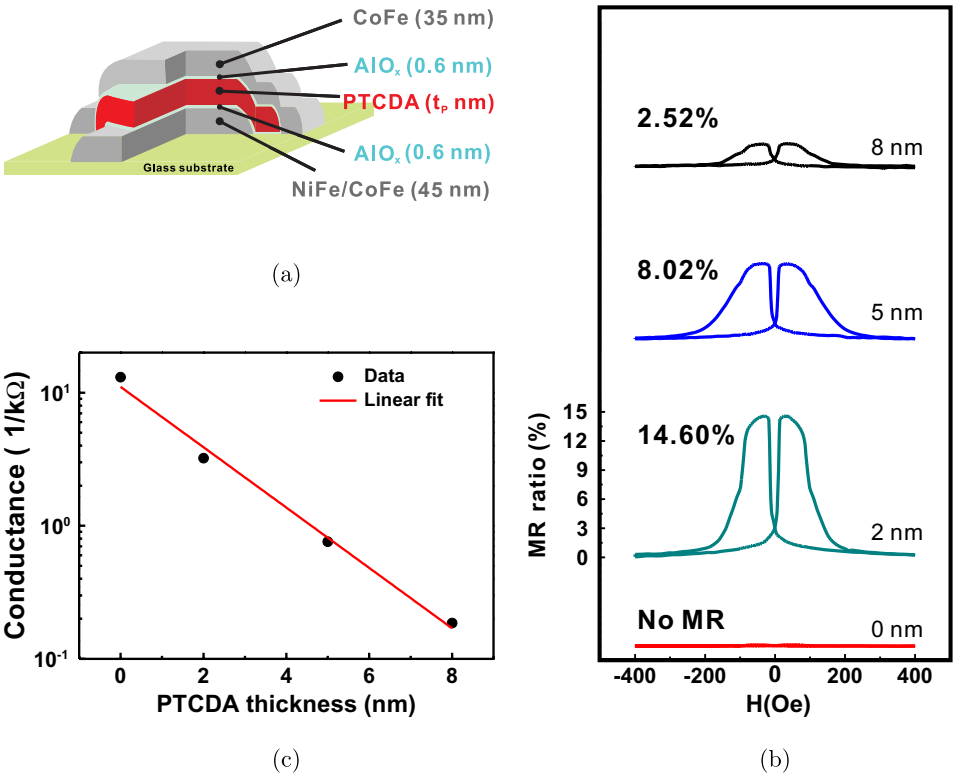

Fig. 1. (a) Schematic diagram of the tri-layered OSV dusted with partially oxidized alumina at the organic–FM interfaces. (b) The room-temperature magnetoresistive curves of OSVs with various PTCDA thicknesses (t_P). The PTCDA-empty ($t_P = 0$) sample exhibits no MR. (c) The junction conductance (G_J) versus t_P plotted in logarithmic scale.

spin-valve type characteristics. An MR ratio (defined as the percentage change of resistance divided by the saturated resistance) of 14.6% is observed in the sample with 2-nm PTCDA, and the ratio decreases rapidly as t_P increases. A PTCDA-empty ($t_P = 0$) test sample exhibits zero MR ratio, indicating that the partially oxidized alumina layer alone cannot form an effective spin-transport barrier. The plot of junction conductance as a function of PTCDA thickness is shown in Fig. 1(c). The exponential dependence implies that the conductance of the OSVs is free from the impact of pinholes or conducting channels formed within the device.

3.2. *Magnetocapacitance*

The OSV can be viewed as a parallel-plate structure and therefore can be modeled by an equivalent circuit that consists of a parallel network of tunneling resistance (R_j) and junction capacitance (C_j), and a spin-independent lead impedance (Z_L) in series [see the inset of Fig. 2(a)].[21] The complex impedance ($Z = R + iX$) of the parallel resistance-capacitance system can then be decomposed into the combination of resistance (R, real part) and reactance (X, imaginary part) as expressed below:

$$R = \frac{R_j}{1 + 4\pi^2 f^2 R_j^2 C_j^2} + R_l, \tag{1}$$

$$X = \frac{-2\pi f C_j R_j^2}{1 + 4\pi^2 f^2 R_j^2 C_j^2} + X_l, \tag{2}$$

where R_j, C_j, R_l, X_l and f stand for the junction resistance, junction capacitance, lead resistance, lead reactance and the test frequency, respectively. The frequency dependence of the imaginary part, measured at both the parallel (P, at 400 Oe) and the antiparallel (AP, at −40 Oe) magnetization states, is shown in Fig. 2(a) for the OSV with $t_P = 2$ nm. The dips of the curves in the high frequency range correspond to the junction resistances of different magnetization states, and the difference is attributed to spin-dependent contribution. By subtracting the two impedance spectra, the spin-independent part can be removed and the resulting spectrum can then be analyzed using the aforementioned RC

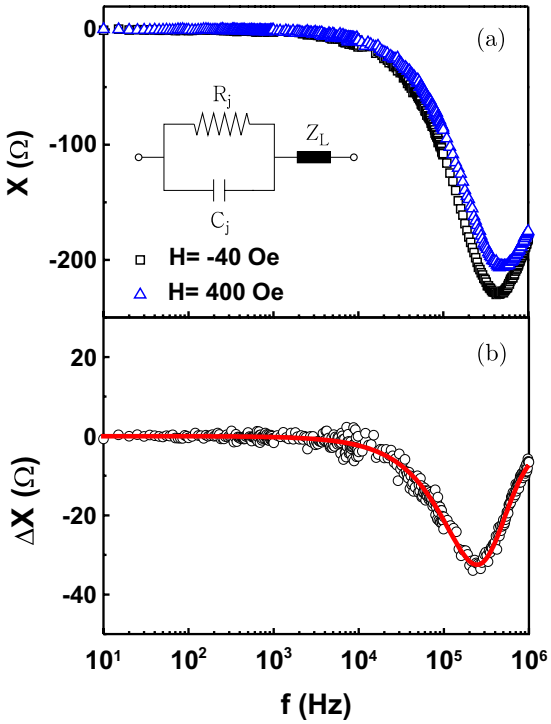

Fig. 2. (a) The imaginary part of impedance versus frequency for PTCDA OSV with $t_P = 2$ nm, measured at 400 Oe (parallel state, open triangles) and −40 Oe (antiparallel state, open squares). The inset shows the schematic of the equivalent RC-circuit model for the OSV. (b) The differential impedance spectrum obtained by subtracting the two spectra in (a). The red curve indicates the best fit using the RC-circuit model (color online).

network model. The difference of the imaginary part of the impedances (ΔX) can be expressed as:

$$\Delta X = -2\pi f\left(\frac{C_m R_m^2}{1+4\pi^2 f^2 R_m^2 C_m^2} - \frac{C_r R_r^2}{1+4\pi^2 f^2 R_r^2 C_r^2}\right), \quad (3)$$

where the subscript "r" denotes a reference state of 400 Oe applied field (P state), and "m" denotes a field condition other than the reference state. To reduce the number of free parameters, R_r is set by the DC-measured junction resistance at 400 Oe. The rest of the parameters, i.e. C_m, R_m and C_r, are determined through the fitting process. The resulting best-fit is indicated by the red curve in Fig. 2(b), which agrees reasonably well with the data (open circles).

By changing the applied magnetic field and repeating the aforementioned fitting process with C_r and R_r held fixed, C_m and R_m of various fields can be obtained. Figures 3(a) and 3(b) plot the MR and

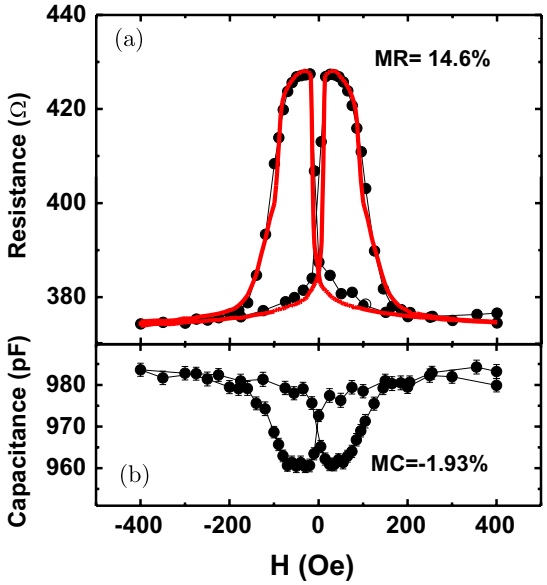

Fig. 3. (a) The MR loop and (b) the MC loop with field variation for PTCDA OSV with $t_P = 2$ nm. The red curve in (a) indicates the MR measured by the DC four-point-probe technique, whereas the solid dots indicate the resulting parameters derived from the model fitting (color online).

MC curves with field variation. As seen in Fig. 3(a), the fitted resistances, indicated by the solid circles, follow the DC-measured MR curve closely. The agreement between the AC fitting and the DC measurement justifies the reliability of the model and the fitting process. Figure 3(b) displays the cycling of the MC response as extracted from the fitting process, which shows an inverse pattern as compared to the MR curve. The MC ratio is defined in the same way as the MR ratio. Table 1 gives the MR and MC ratios for three OSVs with different PTCDA thicknesses. The correlation of MR and MC can be understood by considering the charge density difference at the junction interfaces between the parallel (P) and the antiparallel (AP) states. According to the Jullière model,[26] the junction resistance is lower at P state due to higher probability of electron tunneling through the

Table 1. The MR and MC ratios of PTCDA OSVs with various PTCDA thicknesses (t_P).

t_P (nm)	MR (%)	MC (%)
2	14.6	−1.93
5	8.0	−1.35
8	2.5	−0.44

barrier, leading to higher charge density at the interfaces and hence larger capacitance. On the contrary, at AP state the resistance is larger, the interfacial charge density and the capacitance are lower. The correlation of MR and MC suggests that the geometric capacitance is also governed by spin-dependent transport. Therefore, further characterization of spin-dependent charge accumulation at the junction interfaces is needed.

3.3. *Spin-dependent frequency response*

Figure 4 shows the frequency dependence of the differential impedance (ΔZ) for a series of PTCDA OSVs with different t_P, where the spin-dependent ΔZ spectra are obtained by subtracting the two corresponding impedance spectra measured at

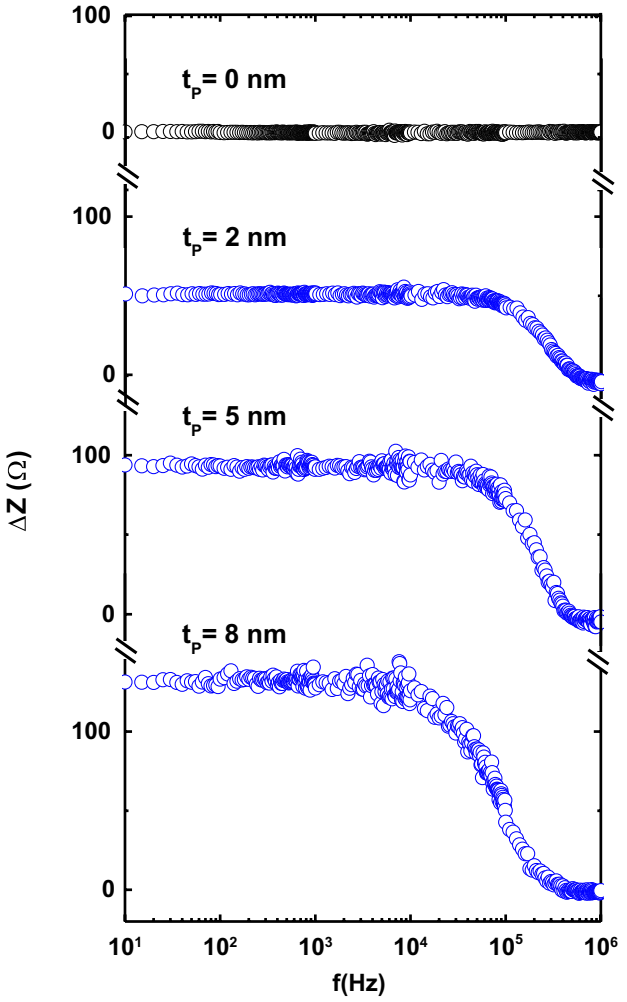

Fig. 4. The differential impedance spectra of PTCDA OSVs with various PTCDA thicknesses (t_P). The PTCDA-empty ($t_P = 0$) sample exhibits zero response.

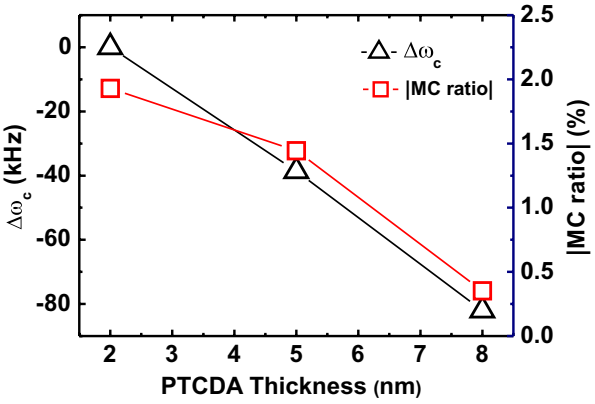

Fig. 5. The shift of critical frequency (black open triangles, referenced to the left vertical axis), and the MC ratios (red open squares, plotted in absolute values, and referenced to the right vertical axis) as functions of PTCDA thickness. (color online).

the P (400 Oe) and AP (−40 Oe) states. The PTCDA-empty sample ($t_P = 0$) shows no magneto-impedance and hence no spin-dependent characteristics. The common feature of the rest of the spectra is a transition from magnetoresistive to magneto-capacitive behavior upon a critical frequency ($\omega_c \approx 1/\mathrm{RC}$). Below ω_c, the impedance response is frequency independent, whereas above ω_c the response is dominated by the capacitive property of the OSV. The critical frequencies for PTCDA OSVs with $t_P = 2\,\mathrm{nm}$, $5\,\mathrm{nm}$ and $8\,\mathrm{nm}$ are around $1 \times 10^5\,\mathrm{Hz}$, $6 \times 10^4\,\mathrm{Hz}$ and $2 \times 10^4\,\mathrm{Hz}$, respectively. If we plot the frequency shift (referenced to the $t_P = 2\,\mathrm{nm}$ sample) with respect to t_P, the result is shown in Fig. 5. The absolute value of the MC ratio is plotted in the same graph, which exhibits a decreasing trend with the PTCDA barrier thickness. In the present study, the MC effect has been characterized by an intrinsic model based on the spin-dependent states, which implies that any spin-induced electronic distribution and interfacial polarization at the FM/OSC interface would impact the effect. The inverse relationship between the size of MC and the spacer thickness suggests a mechanism of charge accumulation at the microscopic interfaces. To characterize the spin-dependent electronic states at the FM/OSC interfaces, further investigation is in progress.

4. Conclusion

In conclusion, we have demonstrated the DC MR and AC MC properties in a series of PTCDA OSVs. The magneto-impedance spectra are fitted to an

equivalent RC-circuit model through which the capacitive parameters are extracted. The process is validated by the agreement between the extracted resistive parameters and the measured MR curves. We have also revealed that the transport of the charge carriers is related to the charge accumulation at the FM/OSC interfaces. Further investigation of the interfacial charge accumulation should provide deeper insights into the transport mechanism in organic spin valves.

Acknowledgments

This work is supported by the National Science Council of Taiwan under Grant No. NSC 100-2120-M-002-002.

References

1. C. W. Tang and S. A. VanSlyke, *Appl. Phys. Lett.* **51**, 913 (1987).
2. J. Shinar and R. Shinar, *J. Phys. D: Appl. Phys.* **41**, 133001 (2008).
3. C. W. Tang, *Appl. Phys. Lett.* **48**, 183 (1986).
4. M. Grätzel, *Nature* **414**, 338 (2001).
5. V. Dediu, M. Murgia, F. C. Matacotta, C. Taliani, and S. Barbanera, *Solid State Commun.* **122**, 181 (2002).
6. I. Bergenti, V. Dediu, E. Arisi, T. Mertelj, M. Murgia, A. Riminucci, G. Ruani, M. Solzi and C. Taliani, *Org. Electron.* **5**, 309 (2004).
7. G. Salis, S. F. Alvarado, M. Tschudy, T. Brunschwiler and R. Allenspach, *Phys. Rev. B* **70**, 085203 (2004).
8. V. A. Dediu, L. E. Hueso, I. Bergenti and C. Taliani, *Nat. Mater.* **8**, 707 (2009).
9. T. D. Nguyen, E. Ehrenfreund and Z. Valy Vardeny, *Science* **337**, 204 (2012).
10. Z. H. Xiong, D. Wu, Z. Valy Vardeny and J. Shi, *Nature* **427**, 821 (2004).
11. T. S. Santos, J. S. Lee, P. Migdal, I. C. Lekshmi, B. Satpati and J. S. Moodera, *Phys. Rev. Lett.* **98**, 016601 (2007).
12. J. H. Shim, K. V. Raman, Y. J. Park, T. S. Santos, G. X. Miao, B. Satpati and J. S. Moodera, *Phys. Rev. Lett.* **100**, 226603 (2008).
13. K.-S. Li, Y.-M. Chang, S. Agilan, J.-Y. Hong, J.-C. Tai, W.-C. Chiang, K. Fukutani, P. A. Dowben and M.-T. Lin, *Phys. Rev. B* **83**, 172404 (2011).
14. K. T. McCarthy, A. Hebard and S. B. Arnason, *Phys. Rev. Lett.* **90**, 117201 (2003).
15. P. Padhan, P. LeClair, A. Gupta, K. Tsunekawa and D. D. Djayapawira, *Appl. Phys. Lett.* **90**, 142105 (2007).
16. H. Kaiju, S. Fujita, T. Morozumi and K. Shiiki, *J. Appl. Phys.* **91**, 7430 (2002).
17. A. M. Sahadevan, K. Gopinadhan, C. S. Bhatia and H. Yang, *Appl. Phys. Lett.* **101**, 162404 (2012).
18. S. Zhang, *Phys. Rev. Lett.* **83**, 640 (1999).
19. S. T. Chui and L. Hu, *Appl. Phys. Lett.* **80**, 273 (2002).
20. G. Landry, Y. Dong, J. Du, X. Xiang and J. Q. Xiao, *Appl. Phys. Lett.* **78**, 501 (2001).
21. Y. M. Chang, K. S. Li, H. Huang, M. J. Tung, S. Y. Tong and M. T. Lin, *J. Appl. Phys.* **107**, 093904 (2010).
22. J. M. Daughton, *J. Appl. Phys.* **81**, 3758 (1997).
23. L. S. C. Pingree, B. J. Scott, M. T. Russell, T. J. Marks and M. C. Hersam, *Appl. Phys. Lett.* **86**, 073509 (2005).
24. P. P. Boix, G. G. Belmonte, U. Muñecas, M. Neophytou, C. Waldauf and R. Pacios, *Appl. Phys. Lett.* **95**, 233302 (2009).
25. J. Y. Hong, K. H. Ou Yang, B. Y. Wang, K. S. Li, H. W. Shiu, C. H. Chen, Y. L. Chan, D. H. Wei, F. H. Chang, H. J. Lin, W. C. Chiang and M. T. Lin, *Appl. Phys. Lett.* **104**, 083301 (2014).
26. M. Jullière, *Phys. Lett.* **54A**, 8 (1975).